J. Fluid Mech. (1985), *vol.* 154, *pp.* 357–375
Printed in Great Britain

Some numerical experiments on developing laminar flow in circular-sectioned bends

By J. A. C. HUMPHREY,
University of California, Berkeley, California

H. IACOVIDES AND B. E. LAUNDER
UMIST, Manchester

(Received 30 July 1984)

The paper reports numerical solutions to a semi-elliptic truncation of the Navier–Stokes equations for the case of developing laminar flow in circular-sectioned bends over a range of Dean numbers. The ratios of bend radius to pipe radius are 7:1 and 20:1, corresponding with the configurations examined experimentally by Talbot and his co-workers in recent years. The semi-elliptic treatment facilitates a much finer grid than has been possible in earlier studies. Numerical accuracy has been further improved by assuming radial equilibrium over a thin sublayer immediately adjacent to the wall and by re-formulating the boundary conditions at the pipe centre.

Streamwise velocity profiles at Dean numbers of 183 and 565 are in excellent agreement with laser-Doppler measurements by Agrawal, Talbot & Gong (1978). Good, albeit less complete, accord is found with the secondary velocities, though the differences that exist may be mainly due to the difficulty of making these measurements. The paper provides new information on the behaviour of the streamwise shear stress around the inner line of symmetry. Upstream of the point of minimum shear stress, our numerical predictions display a progressive shift towards the result of Stewartson, Cebici & Chang (1980) as the Dean number is successively raised. Downstream of the minimum, however, in contrast with the monotonic approach to an asymptotic level reported by Stewartson, the numerical solutions display a damped oscillatory behaviour reminiscent of those from Hawthorne's (1951) inviscid-flow calculations. The amplitude of the oscillation grows as the Dean number is raised.

1. Introduction

The movement of fluid through curved pipes and bends is of considerable practical and fundamental interest. It is well known that in such flows secondary motions arise in the cross-stream planes producing a streamwise flow pattern which may be far removed from that found in a straight pipe. The secondary motions can be explained qualitatively in terms of the response of a viscous-fluid element to an imbalance between the centripetal acceleration and the cross-stream pressure gradient induced by lateral curvature of the main flow; see, for example, Cuming (1952) and Johnston (1978). In a curved pipe, the result is a cross-stream or secondary motion carrying fluid symmetrically along the pipe walls from the outer to the inner line of symmetry and along the symmetry plane of the pipe from the inner to the outer line of symmetry as shown in figure 1.

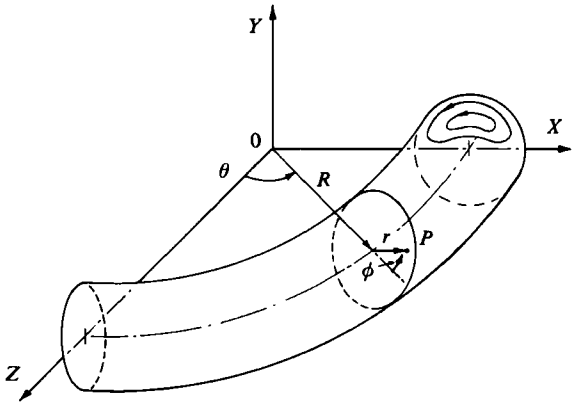

FIGURE 1. The configuration considered and the describing coordinates.

Analysis of the equations describing laminar flow through curved pipes shows that two parameters characterize the flow; the radius ratio $\delta = a/R$ and the Dean number $De = \delta^{\frac{1}{2}} Re$ (Berger, Talbot & Yao, 1983). In the above definitions, a is the radius of the pipe cross-section, R is the pipe mean radius of curvature, and Re is the flow Reynolds number $\overline{W}\, 2a/\nu$ where $\overline{W}$ is the bulk average velocity through the pipe and ν is the fluid kinematic viscosity. Since the Dean number is equal to the ratio of the square root of the product of the inertia and centrifugal forces to the viscous force, it provides a measure of the intensity of the secondary flow. The radius ratio δ is a more direct measure of the influence of pipe geometry on the flow. It affects the balance of inertia, viscous and centrifugal forces. Berger *et al.* (1983) point out that the influence of δ on the flow through curved pipes is not as well understood as that of the Dean number.

Fully developed flow in curved pipes has been the subject of extensive research, a review of the subject having recently been made by Berger *et al.* (1983). The more complex entry flow into a curved pipe has been studied far less completely. Theoretical attempts to solve the problem have been seriously handicapped by a lack of sureness in the simplifying assumptions underlying the various analytical approaches. In addition, for fixed δ and De, the flow developing in a curved pipe is a function of the inlet-plane boundary conditions and these present some difficulties for general values of Re; see Stewartson, Cebeci & Chang (1980) and Berger *et al.* (1983).

Yao & Berger (1975) and Stewartson *et al.* (1980) have investigated the entry-flow-development problem theoretically for $De \gg 1$. In the former case, two sets of equations were derived, one for the inviscid-core flow and the other for the three-dimensional boundary layer. At the inlet plane zero cross-stream-velocity components and a uniform axial velocity were prescribed. Along the pipe wall zero-slip, impermeable conditions were specified. A development of the Kármán–Pohlhausen integral method was used to solve the boundary-layer equations.

A set of boundary-layer equations, equivalent to that of Yao & Berger, was solved numerically by Stewartson *et al.* but core-flow/boundary-layer interactions were neglected. They also prescribed zero cross-stream velocity components at the inlet plane, but they followed Singh (1974) in imposing a potential-vortex condition for the streamwise velocity component. At any fixed streamwise location $R\theta$ the calculation sequence always advanced from $\phi = 0$ at the outer line of symmetry to $\phi = 180°$ at the inner line of symmetry. Use was made of preliminary solutions of

the flow field for all ϕ when $R\theta = 0$ and all $R\theta$ when $\phi = 0$. The Keller box scheme was used to solve partial differential equations for the leading terms in a power-series expansion. The coefficients in the series were obtained *seriatim* and the series summed to yield the preliminary solutions.

Yao & Berger's solution of the boundary-layer flow in a curved pipe predicts that separation of the secondary flow or circumferential boundary layer will take place at a streamwise location from the inlet plane of about $0.01a(De/\delta)^{\frac{1}{2}}$. The width of the separation zone, i.e. the distance between $\phi = 180°$ and the point of separation, was found to increase with streamwise location, tending asymptotically to a maximum value of 54°. This finding is in qualitative agreement with the integral solution for fully developed flow obtained by Barua (1963) who predicts a secondary boundary-layer separation at $\phi = 153°$, but does not accord with either the fully developed integral solution of Ito (1969) or the numerical studies of Collins & Dennis (1975) who do not predict separation. In contrast, and for the first time, Stewartson *et al.* predict a vanishing of the *streamwise* component of skin friction on the inner line of symmetry, $\phi = \pi$, at $R\theta = 0.943a/\delta^{\frac{1}{2}}$. The position of zero shear stress represents a singularity in their calculations since the shear stress increases again immediately past the zero point on the inner line of symmetry. From their study, the authors concluded that the secondary boundary layers 'collide' at $\phi = 180°$ forming a radial jet which takes fluid from the inner to the outer pipe-wall region along the symmetry plane.

Experimental measurements obtained by Agrawal, Talbot & Gong (1978) using the laser-Doppler velocimeter technique in a transparent curved pipe with $\delta = \frac{1}{7}$ suggest that separation of the circumferential boundary layer, in the sense predicted by Yao & Berger, for example, may have occurred by $R\theta = 3.46a/\delta^{\frac{1}{2}}$ for $De = 138$ and by $R\theta = 6.23a/\delta^{\frac{1}{2}}$ for $De = 678$. The values 3.46 and 6.23 are considerably larger than those suggested by either Yao & Berger's analysis (0.12 and 0.26) or the constant 0.943 predicted by Stewartson *et al.* for the position of zero streamwise shear stress. However, it is interesting to note that, for their higher Dean number, Agrawal *et al.* observed a striking modification of the secondary-flow profiles measured in the region of the inside of the bend at two stations: $R\theta = 1.39a/\delta^{\frac{1}{2}}$ and $R\theta = 2.31a/\delta^{\frac{1}{2}}$. Although the authors found it difficult to interpret their results, they associated the phenomenon with some form of separation.

In an effort to verify the finding of Stewartson *et al.* Talbot & Wong (1982) used an electrochemical technique to obtain the wall-shear stress along the inner line of symmetry in a curved pipe with $\delta = \frac{1}{7}$. Measurements were made over the range $188 \leqslant De \leqslant 1622$. They found that the wall shear decreased to a minimum value with increasing De, the minimum being located at $R\theta \simeq 0.96a/\delta^{\frac{1}{2}}$, in close agreement with the value predicted by Stewartson *et al.* Upstream of the minimum the measured wall-shear stress was also in agreement with the predictions by Stewartson *et al.* but on the downstream side substantial discrepancies were found between measurements and predictions. Berger *et al.* point out that the calculations of Stewartson *et al.* are inaccurate beyond the singularity on the inner line of symmetry and must be discounted; further discussion of this point is given by Talbot & Wong (1982).

From the above it is clear that several important aspects of developing curved-pipe flow have not yet been resolved. Analytical methods seeking to model the flow as an inviscid core interacting with a three-dimensional boundary layer lead to asymptotic results that are at variance with numerical calculations of the fully developed form of the Navier–Stokes equations. Analytical models do not yet exist which include the effect of boundary-layer separation on the inviscid-core flow and, more importantly, the very existence of separation is still an unresolved issue.

The arrival of large-core digital computers has made feasible the numerical solution of either the full or some truncated version of the Navier–Stokes equation. Predictions of developing laminar flows in curved pipes by three-dimensional finite-difference procedures have been reported by Patankar, Pratap & Spalding (1974), Rushmore (1975), Liu (1976, 1977), Humphrey (1977) and Levy, Briley & McDonald (1983). The procedure of Patankar *et al.* is based on the boundary-layer equations (with a uniform streamwise pressure gradient applied over each cross-sectional plane) and is thus applicable only to pipes with very large radius ratios. Levy *et al.* also adopt a marching scheme by taking the pressure field from a potential solution with a bulk correction applied plane-by-plane to maintain the same mass flow at any section. While this appears a powerful and economical approach to apply in the early stages of development, the laminar-flow-entry problem was not of principal interest to these workers and consequently no extensive investigation was reported. Moreover, the approach becomes less accurate when there is strong interaction between the viscous and non-viscous regions at high Dean number. The other numerical studies noted above have been based on discretizations of the full Navier–Stokes equations and share in common the problem of false diffusion arising from the use (for stability) of upwind differencing with an inevitably coarse mesh. As a result, flow details such as small secondary eddies tend to be smeared out; none of the studies, for example, has reported separation of the secondary flow.

The present contribution is aimed at throwing some light on the various unresolved phenomena discussed above associated with developing flows in pipe bends. Efforts have been made to reduce numerical errors to unimportant levels by following Pratap & Spalding (1975) in using a semi-elliptic rather than a fully elliptic treatment (thus permitting considerably finer meshes than earlier studies), by adopting the third-order *quadratic* upwind differencing of Leonard (1979) (rather than the usual first-order upwinding) and by removing the numerical singularity at the pipe axis. Although numerical resolution is gradually lost as the Dean number is raised, the results provide evidence of secondary-flow separation – albeit very weak – for De greater than 500. They also show the occurrence of a minimum streamwise wall shear stress on the inner line of symmetry. As the Dean number is successively raised, the minimum value decreases and occurs at progressively smaller values of $R\theta\delta^{\frac{1}{2}}/a$, though, even at the highest value of De considered, this dimensionless position is still approximately twice as far downstream as predicted by Stewartson's analysis.

While preparing the results of the present study for publication, the recent thesis by Soh (1983) on entrance flow in a curved pipe and, subsequently, the paper by Soh & Berger (1984) came to our notice. As in several earlier explorations, these workers had used a fully elliptic discretization. Despite the resultant coarseness of their numerical mesh, by adopting central differencing for convective transport and by carefully arranging their mesh non-uniformly over the domain, a superior level of detail in the solutions was achieved than had hitherto been reported. The present work, which has aimed at providing a very detailed comparison with the experiments of Talbot and his co-workers, includes comparisons with the Soh & Berger study where feasible. We have omitted consideration of those aspects of the flow where our own findings merely confirm Soh & Berger's results.

2. Summary of the numerical solution procedure and boundary conditions

The equations describing the development of a viscous fluid in a toroidal duct such as shown in figure 1 may be written:

continuity

$$\frac{\partial}{\partial \phi} r_c U + \frac{\partial}{\partial r} r r_c V + \frac{\partial}{\partial \theta} r W = 0; \tag{1}$$

momentum

$$\rho[C(\psi) + S_C(\psi)] = D(\psi) + S_D(\psi) + S_p(\psi). \tag{2}$$

In (1), U, V and W denote velocity components in the circumferential ϕ, radial r and streamwise θ directions respectively, $r_c = R + a\cos\phi$ is the local radius from the centre of the bend, while, in (2), ψ stands for any of the velocity components, the associated source and sink terms being given in table 1. The operators $C(\psi)$ and $D(\psi)$ are defined by

$$C(\psi) \equiv (r r_c)^{-1}\left[\frac{\partial}{\partial \phi}(r_c U\psi) + \frac{\partial}{\partial r}(r r_c V\psi) + \frac{\partial}{\partial \theta}(rW\psi)\right], \tag{3}$$

$$D(\psi) \equiv (r r_c)^{-1}\left[\frac{1}{r}\frac{\partial}{\partial \phi}\left(r_c \mu \frac{\partial \psi}{\partial \phi}\right) + \frac{\partial}{\partial r}\left(r r_c \mu \frac{\partial \psi}{\partial r}\right)\right]. \tag{4}$$

We note from (4) that second derivatives with respect to θ are omitted. In consonance with this form of the describing equations a 'semi-elliptic' finite-volume discretization is adopted, a description applied to a solution where only the pressure field is treated as elliptic. The pressure thus requires storing over the whole domain. In contrast, the velocity components are solved in a marching fashion and thus require values to be held only on two adjacent (r, ϕ)-planes of nodes. This type of solution procedure, first introduced by Pratap & Spalding (1975), is particularly attractive in three-dimensional flows for then the savings in memory required for the velocity components (compard to a fully elliptic solution) may allow a sufficiently fine mesh to be used for the pressure field to reduce numerical errors to unimportant levels. The present numerical procedure has broadly followed the strategy of Pratrap & Spalding, but several differences in discretization and organization have been introduced to improve the numerical accuracy of the results. Quadratic upstream interpolation, QUICK, (Leonard 1979) is used to approximate convective transport in the cross-sectional plane of the duct following the conclusions of Huang, Launder & Leschziner (1985) that this was, overall, the most accurate of the simple treatments of convection (see also Han, Humphrey & Launder 1981). Indeed, in tests of flow in a driven square cavity (a flow with generic similarities to the secondary motion generated in the present study) QUICK has been found to achieve better numerical accuracy for a given mesh than central differencing. It is, moreover, relatively free of the stability problems that usually prevent central differencing being applied in other than time-stepping solvers. The pressure/continuity connection is applied by way of Patankar's (1980) SIMPLER algorithm; in preliminary tests this was found to give convergence rates an order of magnitude faster than the earlier and very widely used pressure-correction scheme SIMPLE (Patankar & Spalding 1972).

In the original semi-elliptic scheme of Pratap & Spalding (1975) no in-plane iterations were made on the velocity field and thus, of necessity, coefficients of the difference equations were based entirely on upstream information. Although economical, this practice proved to be inadequate in the present study which has

ψ	$S_C(\psi)$	$S_p(\psi)$	$S_D(\psi)$
U	$\frac{VU}{r}+\left\{\frac{W^2\sin\phi}{r_c}\right\}$	$-\frac{1}{r}\frac{\partial p}{\partial \phi}$	$\frac{1}{r_c}\frac{\partial}{\partial\phi}\left\{r_c\,\mu\left(\frac{\partial U}{\partial\phi}+2V\right)\right\}+\frac{1}{rr_c}\frac{\partial}{\partial r}\left\{r_c\,\mu\left(\frac{\partial V}{\partial\phi}-U\right)\right\}$ $+\mu\frac{\partial}{\partial r}\left\{\frac{U}{r}\right\}+\frac{\mu}{r^2}\frac{\partial V}{\partial\phi}+\frac{1}{r}\frac{\partial}{\partial\theta}\left\{\mu\frac{\partial}{\partial\phi}\left(\frac{W}{r_c}\right)\right\}$ $-\frac{2\mu\sin\phi}{r_c^2}\left\{U\sin\phi-V\cos\phi-\frac{\partial W}{\partial\theta}\right\}$
V	$-\left\{\frac{\cos\phi\,W^2}{r}\right\}-\left\{\frac{U^2}{r}\right\}$	$-\frac{\partial p}{\partial r}$	$\frac{1}{r_c}\frac{\partial}{\partial\phi}\left\{r_c\,\mu\frac{\partial}{\partial r}\left(\frac{U}{r}\right)\right\}+\frac{1}{rr_c}\frac{\partial}{\partial r}\left\{rr_c\,\mu\frac{\partial V}{\partial r}\right\}$ $-\frac{2\mu}{r^2}\left\{\frac{\partial U}{\partial\phi}+V\right\}+\frac{1}{r}\frac{\partial}{\partial\theta}\left\{r\mu\frac{\partial}{\partial r}\left(\frac{W}{r_c}\right)\right\}$ $+\frac{2\mu\cos\phi}{r_c^2}\left\{U\sin\phi+V\cos\phi-\frac{\partial W}{\partial\theta}\right\}$
W	$-\left\{\frac{\sin\phi\,UW}{r_c}\right\}$ $+\left\{\frac{\cos\phi\,VW}{r_c}\right\}$	$-\frac{1}{r_c}\frac{\partial p}{\partial\theta}$	$\frac{1}{rr_c}\frac{\partial}{\partial\phi}\left\{\mu\left(\frac{\partial U}{\partial\theta}+W\sin\phi\right)\right\}$ $+\frac{1}{rr_c}\frac{\partial}{\partial r}\left\{2\mu\left(\frac{\partial V}{\partial\theta}-W\cos\phi\right)\right\}$ $+\frac{1}{r_c^2}\frac{\partial}{\partial\theta}\left\{\mu\left(\frac{\partial W}{\partial\theta}-2U\sin\theta+2V\cos\phi\right)\right\}$ $-\frac{\mu\sin\phi}{r}\frac{\partial}{\partial\phi}\left(\frac{W}{r_c}\right)+\mu\cos\phi\frac{\partial}{\partial r}\left(\frac{W}{r_c}\right)$ $-\frac{\mu r\sin\phi}{r_c^2}\frac{\partial}{\partial\theta}\left(\frac{U}{r}\right)-\frac{\mu\cos\phi}{r_c^2}\left(\frac{\partial V}{\partial\theta}\right)$

TABLE 1. Source terms for dependent variables

included tighter bends than those examined by Pratap & Spalding† and where, as a result, streamwise variations are more rapid. As the pressure field, which was iterated by repeated streamwise sweeps over the solution domain, approached convergence, first one and finally two in-plane iterations on the velocity field were made with all coefficients being re-evaluated using the current plane information.

At the highest Dean numbers a significant economy in the memory required at any cross-sectional plane was achieved by assuming that the static pressure within a thin annular ring adjacent to the pipe wall was obtainable from radial momentum equilibrium. Within this sub-region, which extended from the wall to $0.9a$, the pressure was obtained from the following degenerate form of the radial momentum equation:

$$\frac{1}{\rho}\frac{\partial p}{\partial r}=\frac{W^2\cos\phi}{r}+\frac{U^2}{r}, \tag{5}$$

while the radial velocity V was obtained from the continuity equation, (4). This parabolic-sublayer treatment (PSL) was originally developed to facilitate the study of complex *turbulent* flows (Iacovides & Launder 1984) but it has also proved helpful

† The Pratap–Spalding study was confined to square-sectioned bends.

for the flows examined here since, at entry to the solution domain, the boundary layer is extremely thin and a fine near-wall mesh is inevitably required.

There is no intrinsic need for a particularly fine mesh at the pipe centre. Many earlier numerical treatments, however, have put radial gradients of all dependent variables to zero at $r = 0$ and, to keep the harmful consequences of this clearly incorrect prescription to unimportant levels, a refined grid has been needed in the vicinity of $r = 0$. The central difficulty is that at $r = 0$ ($J = 1$) there are many coincident nodes each corresponding to a different circumferential angle $\phi(I)$. In the present study, for the streamwise velocity component W the same value has been assigned to all these coincident centre nodes ($W(I, 1)$), this value being the average value over the surrounding nodes:

$$W(I,1) = \sum_{I=2}^{NI-1} \frac{W(I,2)}{(NI-2)},$$

where $I = 2$ and $I = (NI-1)$ correspond to 0 and π radians respectively. The U and V components, however, cannot take the same value at the centre. Instead, it is required that the resultant of $U(I, 1)$ and $V(I, 1)$ should produce the same velocity vector irrespective of the circumferential location. Now this resultant velocity must lie on the symmetry axis: its value V_{res} is obtained as the mean of the radial velocity components on $\phi = 0$ and $\phi = \pi$ on either side of the centre node.† The U and V velocity components for other values of ϕ are then obtained as

$$U(I,1) = V_{\text{res}} \sin\phi; \quad V(I,1) = V_{\text{res}} \cos\phi.$$

Soh & Berger (1984) have also adopted this treatment for finding U and V at the pipe centre.

At the tube wall all three velocity components are set to zero. At the inlet plane the streamwise velocity is assigned as uniform over the plane while the other velocity components are set to zero. At the $\theta = 180°$ plane no constraints are required on the velocity components (which are treated in a boundary-layer fashion) while the streamwise pressure gradient has been set uniform over the section at a level needed to satisfy continuity. This latter condition, while not in accord with the actual pressure gradient at 180° (which is affected by bend-exit effects) has been found to affect the flow pattern only within 20° of the exit (for $\delta = \frac{1}{7}$). None of the comparisons drawn below relates to a position in the bend greater than 160° from the entry.

A number of computations reported below have been repeated several times with different distributions of nodes in the three coordinate directions and with a progressive mesh refinement. The standard mesh density employed was 20 (radial) × 20 (circumferential, ϕ) × 150 (axial, θ) for the pressure p, and for the velocities $28 \times 20 \times 2$. The difference in the number of radial nodes for the velocity and pressure fields arises from the fact that in the 'parabolic sublayer' pressure nodes are not required but velocity nodes are.

The computations have been made on a CDC7600 computer at the University of Manchester Regional Computing Centre. Central processor time required to proceed from a uniform guessed initial pressure field to a final converged state where residual mass errors *summed over the entire domain* were below 0.1 % of the entering mass flow ranged from 10000 s for $De = 138$ to 25000 s for $De = 2712$, for $\delta = \frac{1}{7}$.

† In fact, V_{res} is the average of V on $\phi = 0$ and the *negative* of that on $\phi = \pi$.

3. Presentation and discussion of results

Comparison is drawn first with two experiments reported by Agrawal *et al.* (1978), one in a bend with $\delta = \frac{1}{7}$ at a Dean number of 183 ($Re = 484$) and the other with $\delta = \frac{1}{20}$ and $De = 565$ ($Re = 2530$). In the experiments, the bend was preceded by a bell-mouth entry; the computer stimulation began with a uniform streamwise velocity and zero secondary velocities at the entry plane to the bend (0°). It will be seen later from a comparison with wall stresses that the unavoidable mismatch between the experimental and computational starting profiles leads to a lag in the computation by approximately 5° of arc in the case of $\delta = \frac{1}{7}$. Streamwise-velocity profiles at representative stations are shown for these two flows in figures 2 and 3. Owing to the difference in refractive index between the Perspex pipe and the glycerin–water mixture which provided the working fluid, experimental velocity traverses were made along the non-parallel lines indicated in the figures. The numerical data were interpolated to extract velocities along the same lines.

Near the bend entry the potential vortex is clearly evident in each case. For the lower Reynolds number there is some indication that the measured boundary layer is a little thicker than that computed, in part due to neglect in the computations of any boundary layer at the entry plane. As the shear flow develops around the bend, the secondary motion displaces the velocity maximum to the outside of the bend and, in the case of the higher Dean number, produces double velocity maxima along some lines. The computations and the experiments generally produce a strikingly similar behaviour. The somewhat smaller distortion of the computed profiles at $De = 183$ and $L/R = 7.34$ (where L is the distance from the bend entry measured along the circular path through the pipe centre) compared with experiment is, we believe, probably due to the thinner computational inlet boundary layer. Other small differences that a close examination reveals are probably attributable to the uncertainty in the measured Reynolds number of $\pm 8\%$.

The secondary-flow data reported by Agrawal *et al.* (1978) were in fact obtained later than the streamwise velocities and at different Dean numbers, 138 and 678. Figures 4 and 5 draw comparisons between the measured profiles and the corresponding numerical results. In each case, the secondary flow carries fluid from the outside to the inside of the bend near the wall with a slow return flow over the remainder of the cross-section. At the higher Dean number (or, rather, Reynolds number) the near-wall current is confined closer to the wall due to the thinner streamwise boundary layer and the return-flow pattern is noticeably more complex near the inside of the bend. The numerical computations mirror the experimental data reasonably well but not, it must be acknowledged, as well as in the case of the streamwise profiles discussed above. The predicted near-wall outer-to-inner flow is thicker than that measured. This superficially might appear to arise from numerical diffusion but the QUICK scheme adopted for convection is accurate up to third order and does not suffer from the severe numerical smearing to which upwind differencing is prone. Moreover, grid refinement produced negligible changes in the results at these Dean numbers. The question thus arose as to whether the experimental Dean number could have been different from that reported.† Without claiming to answer that question it is at least of interest to notice that in figure 5 the computed secondary flows at a Dean number twice that reported experimentally are in significantly closer accord with the experiment than the reported value of 678. At this higher Dean

† Professor Talbot advises us that the uncertainty in determining the Dean number in these experiments did not exceed about 10%.

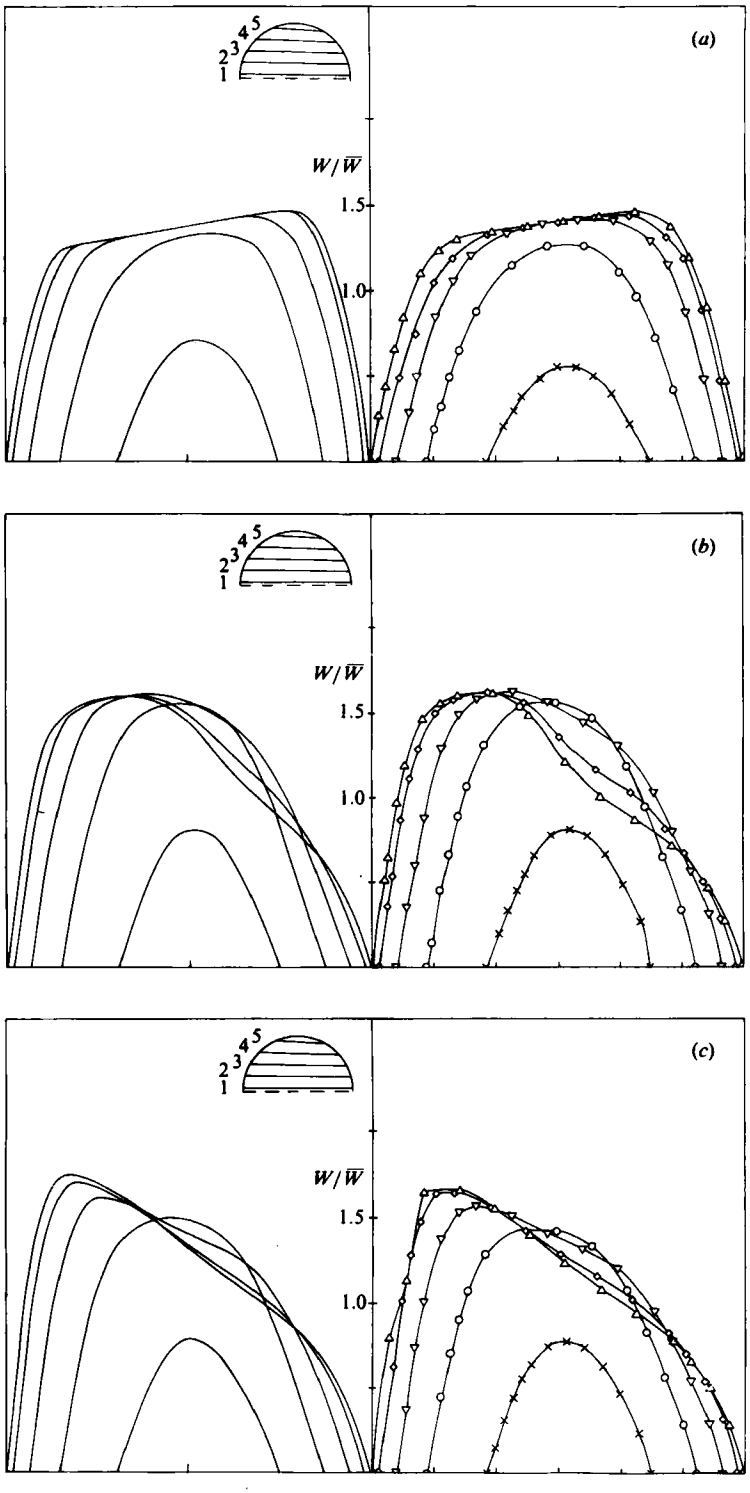

FIGURE 2. Streamwise velocity profiles along lines 1–5. Right-hand figures: experiments of Agrawal *et al.* (1978). Left-hand figures: present computations; $De = 183$; $R/a = 7$. (*a*) $L/a = 1.84$; (*b*) 7.34; (*c*) 19.54.

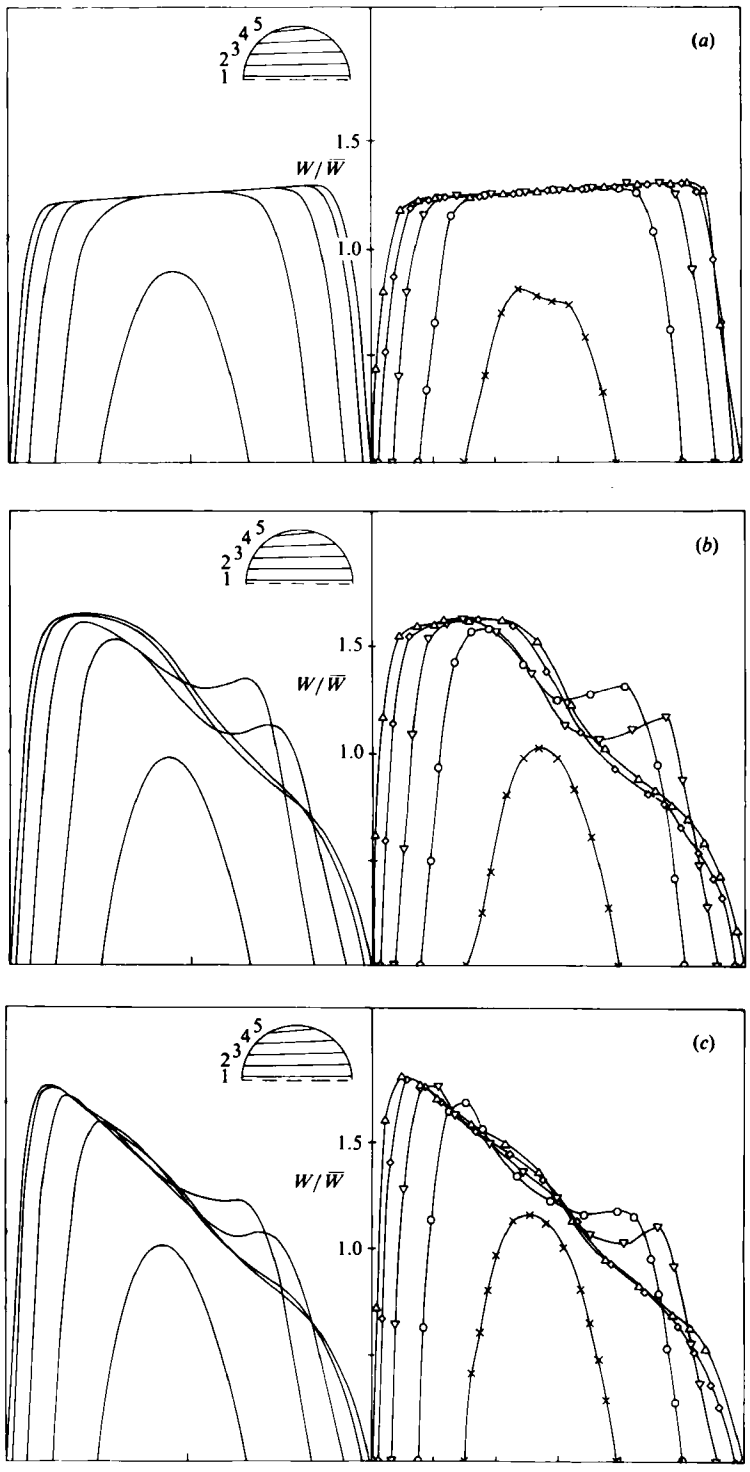

FIGURE 3. Streamwise velocity profiles along lines 1–5. Right-hand figures: experiments of Agrawal *et al.* (1978). Left-hand figures: present computations; $De = 683$; $R/a = 20$. (*a*) $L/a = 2.4$; (*b*) 29.4; (*c*) 57.6.

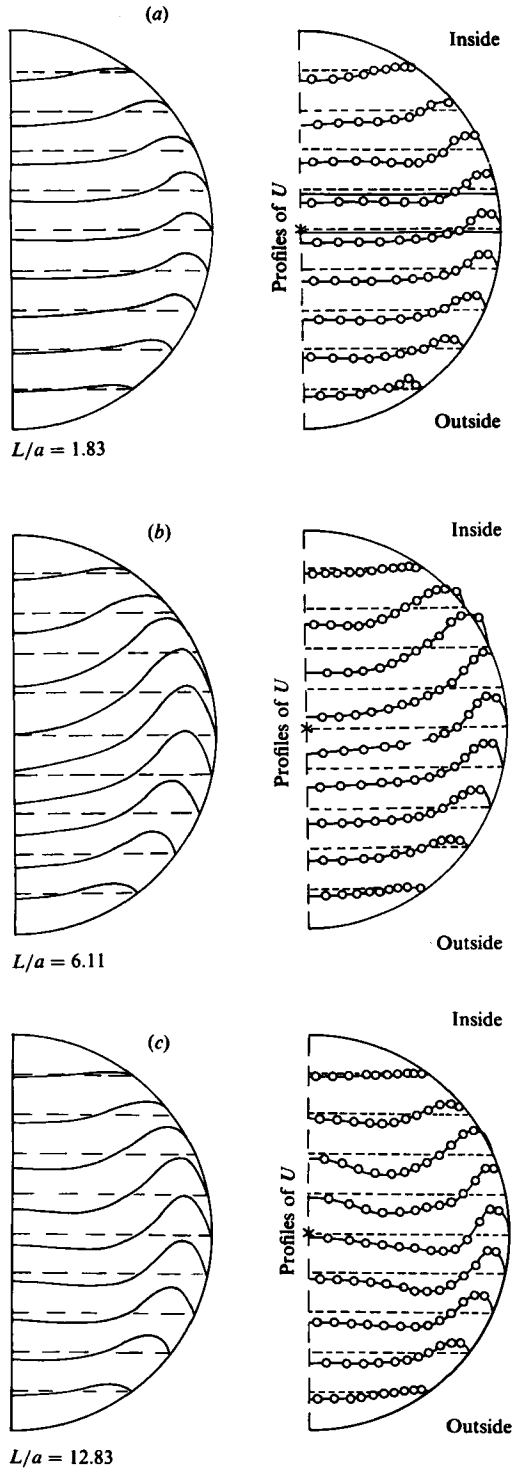

FIGURE 4. Secondary-velocity profiles. Right-hand figures: experiments of Agrawal *et al.* (1978) Left-hand figures: present computations; $De = 138$; $R/a = 7$. (*a*) $L/a = 1.83$; (*b*) 6.11; (*c*) 12.83.

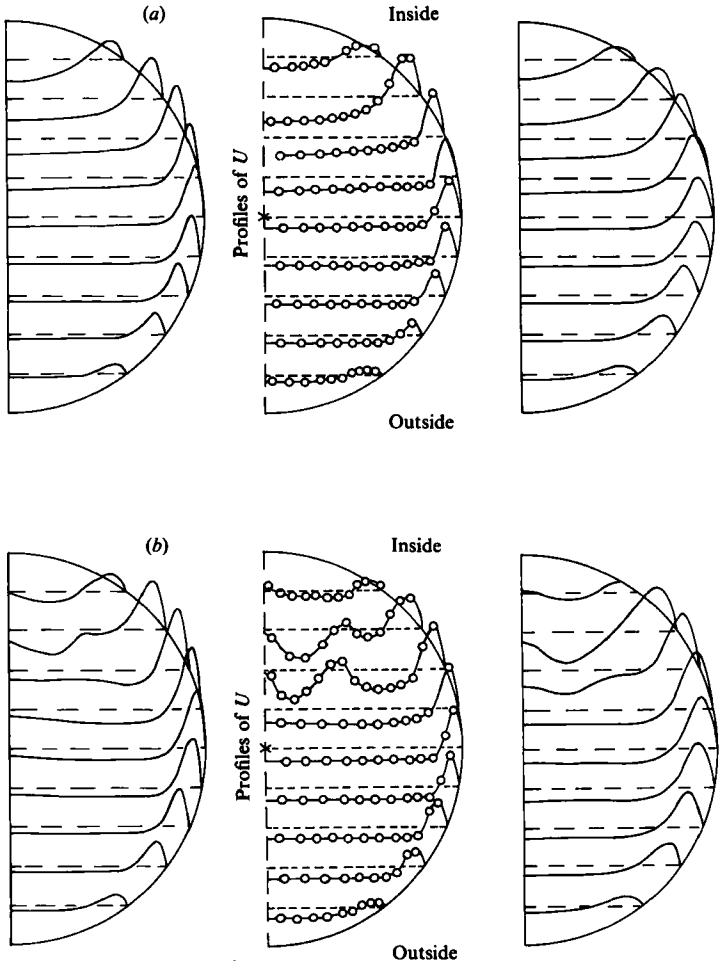

FIGURE 5(a,b). For caption see facing page.

number the secondary profiles reflect the weakening of viscous effects compared to inertial terms through the appearance of secondary maxima and minima along a number of traverse lines near the inside of the bend. Indeed, the computations at $De = 1356$ indicate in figure 5(c) a reversal of the direction of secondary flow on the symmetry plane, implying the formation of a counter-rotating eddy.† In the experiments the secondary velocity on the axis is reduced almost to zero along two traverse lines in figure 5(c) but does not actually reverse. It may be noted, however, that the measured secondary velocities appear to suffer from an 'outward' bias. That is to say, the secondary-flow profiles indicate a mass flow rate to the outside of the bend that is up to 6 times larger than that to the inside. If the flow were fully developed in the axial direction, continuity would require precisely the same inward and outward flow rates along every line drawn from the boundary to the symmetry plane. Now, the predicted secondary profiles *do* indicate that such a balance exists within about 10 %. Thus, in the computations the effects of changes of W in the axial

† It is interesting to note that Azzola & Humphrey (1984) have measured such a counter-rotating eddy near the symmetry plane for *turbulent* flow in a 180° bend.

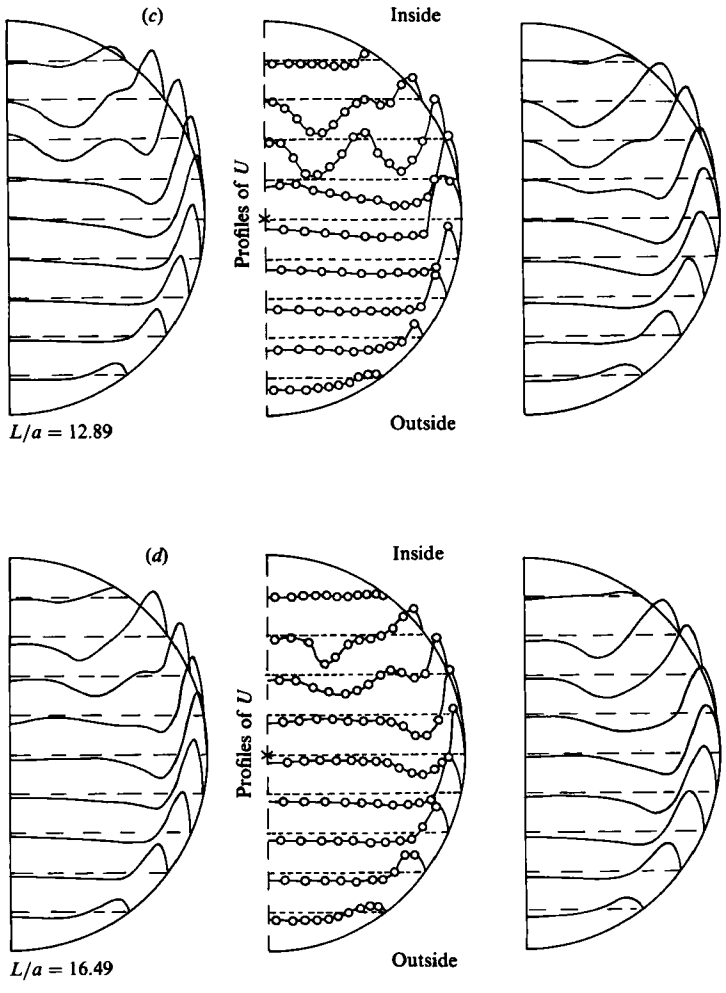

FIGURE 5. Secondary-velocity profiles. Centre figures: experiments of Agrawal *et al.* (1978), $De = 678$. Right-hand figures: present computations, $De = 678$. Left-hand figures: present computations, $De = 1360$. (*a*) $L/a = 3.67$; (*b*) 9.16; (*c*) 12.89; (*d*) 16.49.

direction do not make a major contribution to the mass balance. Now, since there is such close agreement between the measured and computed W profiles, we may infer that in the experiments also the contribution of $\partial(rW)/\partial\theta$ to the mass balance is small beyond the initial entry region. It is thus difficult not to conclude that the experiments, for whatever reason, have given a spurious augmentation of the secondary velocity towards the outside of the bend. Thus it seems probable that the actual flow does indeed exhibit a secondary-flow reversal on the axis. Although the computations – even those at $De = 1356$ – do not quite show the roller-coaster appearance of the experimental profiles, in view of the above discussion the agreement is probably satisfactory.

Agrawal *et al.* (1978) speculated that 'separation' of the secondary flow may have occurred at their data collection point closest to the inside of the bend. In fact, though one cannot distinguish it in the figure, the computed wall-adjacent velocities at this position do take very small negative values as may be inferred from the variation

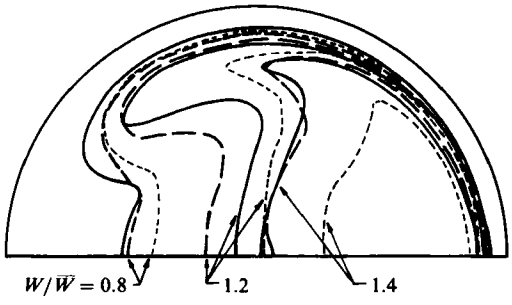

FIGURE 6. Streamwise-velocity contours: $De = 565$; $R/a = 20$; $L/a = 29.4$; ——, Talbot *et al.* experiments; – – – –, present computations; - - - - - - - -, Soh (1983).

of circumferential shear stress in figure 10. Readers are referred to Soh & Berger's plots of the secondary-flow vectors (figures 9 and 10) which also convey clearly the increasing complexity of the secondary-flow pattern with Dean number.

We return briefly to the streamwise-velocity component to observe how its isovels are distorted by the secondary flow field. Figure 6 presents measured and predicted contours for a Dean number of 565 at 83° from the bend entry. Soh (1983) provides computed results for this flow condition at the same location and his predictions are included in the figure. The contour plots convey a clear impression of how the secondary flow (similar to that shown in figure 6*c*) pulls out the axial contours as fluid flows along the walls from the outside to the inside of the bend. Because the bulk of the return flow also takes place along the periphery of the pipe, however, the profiles are folded back on themselves forming hook-like contours or 'fingers'. The present numerical results mimic closely the measurements while Soh's coarse-grid calculations yield contours for $W/\overline{W}$ enclosing smaller regions of the flow than either the measurements or the present calculations; the main features of the flow are nevertheless quite well predicted.

Figures 7–10 relate to the distributions of wall shear stress around the inside of the bend, a topic that has been the main concern in the papers by Stewartson *et al.* (1980) and Talbot & Wong (1982). Figure 7 shows the development of the axial wall shear stress along the inner line of symmetry at four Dean numbers. The predicted behaviour for $De = 678$ is almost identical with that reported by Soh & Berger (1984) for $De = 680.3$. Figure 7 also includes the behaviour predicted by Stewartson *et al.* As discussed in § 1 the analysis developed by these workers gives a vanishing shear stress at $Z \equiv \theta(R/a)^{\frac{1}{2}} = 0.943$ which represents a point of singularity in the solution since immediately downstream therefrom the shear stress rises sharply and then approaches monotonically an asymptotic value. Stewartson *et al.* comment that their analysis is strictly applicable only for very small values of δ and for $De \gg 1$. Certainly, as the Dean number is successively raised the present numerical results shift *in the direction of* that limit, i.e. the minimum dimensionless wall shear rate falls as De increases and the minimum value occurs at progressively smaller values of Z (though even at $De = 2712$ the minimum is reached about twice as far downstream as the predicted singular point). Downstream of the minimum, the numerical solutions display a damped oscillatory behaviour, the amplitude growing as the Dean number is raised. This behaviour is evidently in striking contrast with Stewartson's result, yet is at least in qualitative agreement with the inviscid analysis of Hawthorne (1951).

It would have been interesting to extend the numerical results to higher Dean numbers but this was not feasible since to achieve sensible grid independence for larger

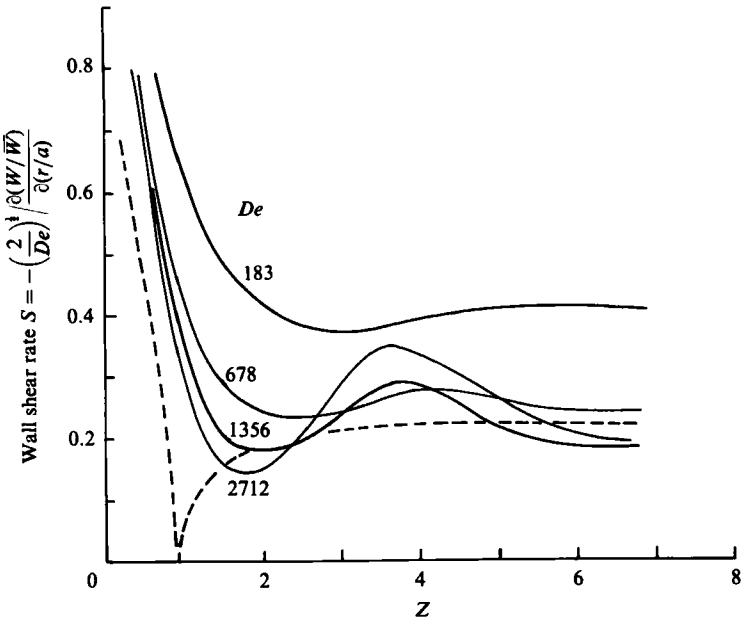

FIGURE 7. Distribution of dimensionless wall shear stress along inner line of symmetry: ——, present computations; – – – –, Stewartson *et al.* (1980).

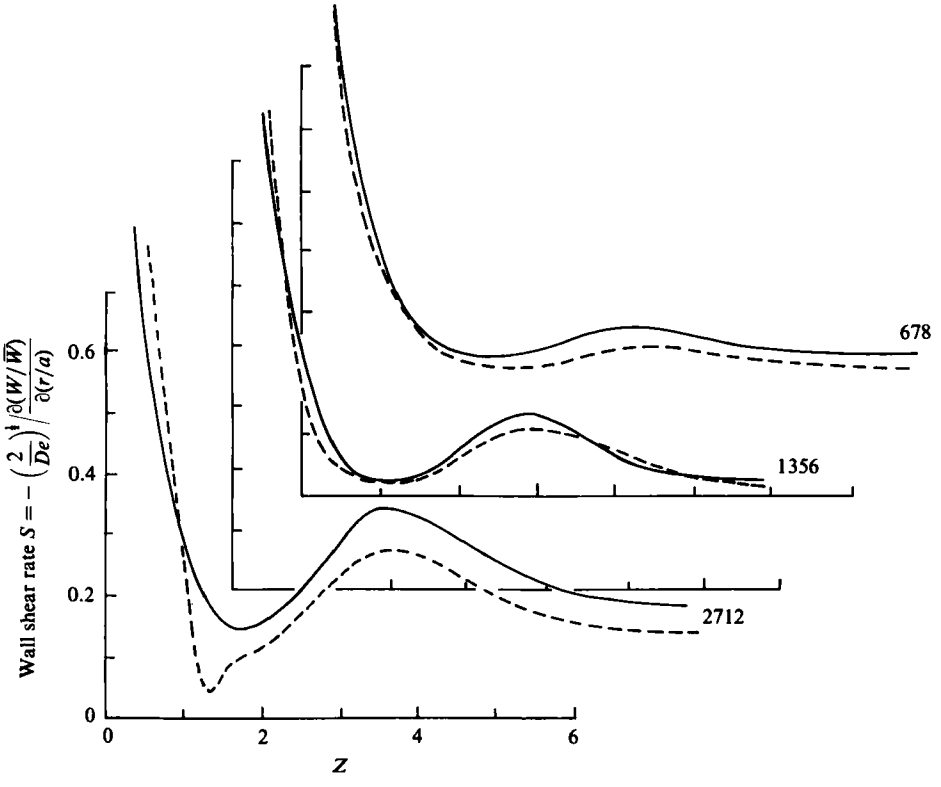

FIGURE 8. Distribution of dimensionless wall shear stress along inner line of symmetry. Sensitivity of results to grid refinement: ——, $28 \times 20 \times 150$ nodes; – – – – –, $20 \times 20 \times 100$ nodes.

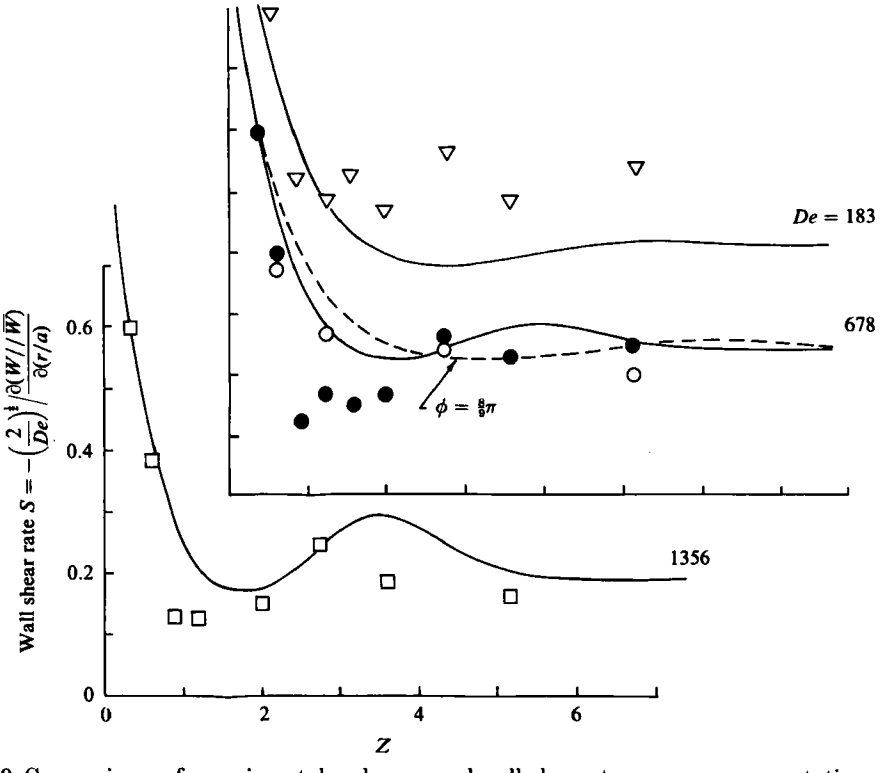

FIGURE 9. Comparisons of experimental and measured wall-shear stresses ——, computations along $\phi = \pi$; ▽, ●, □ experiments, Talbot & Wong $\phi = \pi$; – – – –, computations along $\phi = \frac{8}{9}\pi$; ○, experiments $\phi = \frac{8}{9}\pi$.

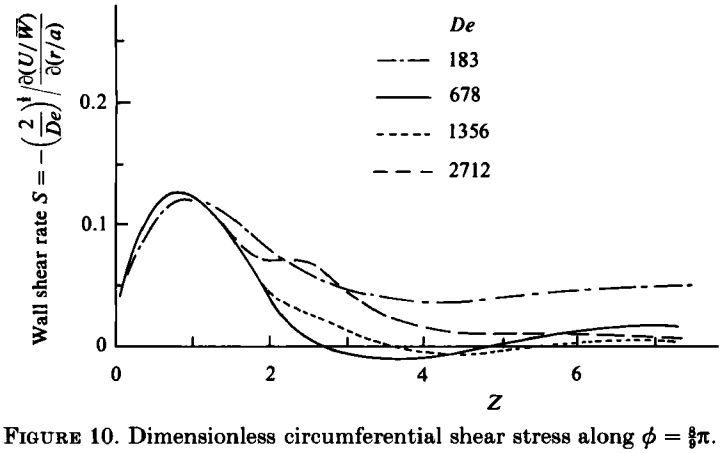

FIGURE 10. Dimensionless circumferential shear stress along $\phi = \frac{8}{9}\pi$.

De than those reported would have required finer meshes – and thus more in-core storage than was available to us. The effect of grid refinement on the present solutions can be judged from figure 10 which shows results obtained for the three highest Dean numbers with the standard $28 \times 20 \times 150$ grid and with a coarser version: $20 \times 20 \times 100$. At Dean numbers of 678 and 1356 the changes in shear stress arising from grid refinement are rather small and the trend is generally to raise the shear stress slightly. The change is more substantial at the highest Dean number, the

minimum shear stress being raised by a factor of 3. For this last case the coarser grid gives a behaviour up to the position of minimum shear stress much closer to that predicted by the analysis of Stewartson *et al.* Nevertheless, the finer grid solution brings the behaviour at this highest Dean number much more into line with the numerical results at lower values of De.

The conclusion that the solution of Stewartson *et al.* did not adequately describe the flow downstream of the singularity was originally drawn by Talbot & Wong (1982) on the basis of experimental shear-stress data obtained by an electrolytic method. Comparisons with these measurements are shown in figure 9 where the present computational curves are all displaced to the left a dimensionless distance 0.2 (corresponding to 4.3° of arc), an arbitrary adjustment to try and account for the effects of the inlet contraction. For $De = 678$ the computed curve corresponding to the streamwise wall stress at $\frac{8}{9}\pi$ is also included to allow comparison with the resultant stress along this line measured by Choi, Talbot & Cornet (1979).† Agreement between the experimental and numerical results is somewhat mixed. At a Dean number of 183 the computed values are some 20% below the data, while at the higher Dean numbers the cluster of data points around $Z = 1.0$ give substantially lower values than predicted. It is hard to ascribe a level of accuracy to the experiments: the calibration curve from Talbot & Wong suggests that the stress levels are systematically low by an amount ranging from 15–25% depending on the surface strain rate, though no estimates of other uncertainties are provided. Apart from the case of the lowest Dean number the impression conveyed by the data seems to be that they scatter about the numerical predictions rather than display conclusive differences. Talbot & Wong inferred from a comparison of their measurements with those at $\frac{8}{9}\pi$ from Choi *et al.* (1979) that the circumferential wall-shear stress at this position was much smaller than the streamwise stress – a conclusion which conflicted with the predicted behaviour of Stewartson *et al.* The present study provides strong support for Talbot & Wong's conclusion. The circumferential stress along $\frac{8}{9}\pi$, shown in figure 10, is an order of magnitude smaller than the streamwise component except in the vicinity of its maximum value. We note that the streamwise variation of this component is essentially independent of Dean number as far as $Z = 1.5$. Moreover, weakly negative values of circumferential shear stress occur for $De = 678$ in the range $2.7 \leqslant Z \leqslant 4.8$ and for $De = 1356$ in the range $3.7 \leqslant Z \leqslant 5.4$. At the highest Dean number the secondary shear stress remains positive, though close to zero for $Z > 4$. It ought to be said that this last result is not conclusively established since it is possible that a further major grid refinement, while producing negligible changes to the streamwise or secondary velocity field, could nevertheless change the circumferential stress from a very weak negative value to an equally weak positive value – or vice versa.

4. Conclusions

Careful numerical solutions have been obtained of several laminar flows developing in 180° bends of circular cross-section that have been the subject of laser-Doppler studies by Talbot and his colleagues. Given the small but unquantifiable mismatch between the computational and the experimental entry conditions, agreement between computed and measured streamwise profiles for Dean numbers of 183 and 565 is extremely close. There is less complete agreement with the secondary velocity

† Because the circumferential stress at this position is small compared to the axial stress, the resultant stress does not differ from the axial value by more than 1%.

profiles and one possibility, that would be consistent with the present results, would be that the experimental data (which were obtained in a separate study from the streamwise profiles) were at a higher Dean number than reported.

The present computational results indicate a gradual approach towards the initial-region behaviour predicted by Stewartson *et al.* (1980) as the Dean number is raised. Even at a Dean number of 2712, however, there are still marked differences from Stewartson's solution. Downstream of the point of minimum shear stress on the inside wall the numerical results indicate an oscillatory development of the streamwise wall stress, the overshoot increasing as the Dean number is raised. This behaviour, which is at least in qualitative agreement with the data of Talbot & Wong (1982), and inviscid-flow calculations of the secondary flow by Hawthorne (1951), is in striking contrast with the predictions of Stewartson *et al.* (1980) which show a monotonic approach to steady-state conditions.

The work has formed part of a collaborative Berkeley–UMIST research programme on (mainly turbulent) flow around 180° bends funded by the US Office of Naval Research through grants N00014-80-C-0031 and N00014-83-G-0021.

Numerical results were generated by a CDC7600 computer at the University of Manchester Regional Computing Centre. Special thanks are due to Professor L. Talbot for his assistance in interpreting the data and his interest and encouragement throughout the project. Authors' names appear alphabetically.

REFERENCES

Agrawal, Y., Talbot, L. & Gong, K. 1978 Laser anemometer study of flow development in curved pipes. *J. Fluid Mech.* **85**, 497–518.

Azzola, J. & Humphrey, J. A. C. 1984 Developing turbulent flow in a 180° curved pipe and its downstream tangent. In *2nd Int. Symp. on Applications of Laser Anemometry to Fluid Mechanics, Lisbon.*

Barua, S. N. 1963 On secondary flow in stationary curved pipes. *Q. J. Mech. Appl. Maths* **16**, 61–77.

Berger, S. A., Talbot, L. & Yao, L.-S. 1983 Flow in curved pipes. *Ann. Rev. Fluid Mech.* **15**, 461–512.

Choi, U. S., Talbot, L. & Cornet, I. 1979 Experimental study of wall shear rates in the entry region of a curved tube. *J. Fluid Mech.* **93**, 465–489.

Collins, W. & Dennis, S. C. R. 1975 The steady motion of a viscous fluid in a curved tube. *Q. J. Mech. Appl. Maths* **28**, 133–156.

Cuming, H. G. 1952 The secondary flow in curved pipes. *Aero. Res. Counc. Rep. Mem. No.* 2880.

Han, T. Y., Humphrey, J. A. C. & Launder, B. E. 1981 A comparison of hybrid and quadratic-upstream differencing in high Reynolds number elliptic flows. *Comp. Meth. Appl. Mech. Engng* **29**, 81.

Hawthorne, W. R. 1951 Secondary circulation in fluid flow. *Proc. R. Soc. Lond.* A **206**, 374–387.

Huang, P. G., Launder, B. E. & Leschziner, M. A. 1985 Discretization of non-linear convection processes: A broad range comparison of four schemes. To appear in *Comp. Meth. Appl. Mech. Engng.*

Humphrey, J. A. C. 1977 Numerical calculation of developing laminar flow in pipes of arbitrary curvature radius. *Can. J. Chem. Engng* **56**, 151–164.

Iacovides, H. & Launder, B. E. 1984 PSL – An economical approach to the numerical analysis of near-wall elliptic flow. *Trans. ASME* I: *J. Fluid Engng* **106**, 245.

Ito, H. 1969 Laminar flow in curved pipes. *Z. angew. Math. Mech.* **49**, 653–663.

Johnston, J. P. 1978 Internal flows. In *Turbulence* (ed. P. Bradshaw). Topics in Applied Physics, vol. **12**, chap. 3. Springer.

LEONARD, B. P. 1979 A stable and accurate convective modelling procedure based on quadratic upstream interpolation. *Comp. Meth. Appl. Mech. Engng* **19**, 59.

LEVY, R., BRILEY, W. R. & MCDONALD, H. 1983 Viscous primary/secondary flow analysis for use with non-orthogonal coordinate systems. *AIAA Paper* 83–056.

LIU, N.-S. 1976 Finite-difference solution of the Navier-Stokes equations for three-dimensional internal flow. In *Proc. 5th Intl Conf. on Num. Meth. in Fluid Dynamics*, pp. 330–335.

LIU, N.-S. 1977 Developing flow in a curved pipe. *INSERM-Euromech 92* **71**, 53–64.

PATANKAR, S. V. 1980 *Numerical Heat Transfer and Fluid Flow*. Hemisphere Publishing Corp./ McGraw-Hill.

PATANKAR, S. V., PRATAP, V. S. & SPALDING, D. B. 1974 Prediction of laminar flow and heat transfer in helically coiled pipes. *J. Fluid Mech.* **62**, 539–551.

PATANKAR, S. V. & SPALDING, D. B. 1972 A calculation procedure for heat, mass and momentum transfer in three-dimensional parabolic flows. *Int J. Heat Mass Transfer* **15**, 1787.

PRATAP, V. S. & SPALDING, D. B. 1975 Numerical computations of the flow in curved ducts. *Aero. Quart.* **26**, 219–228.

RUSHMORE, W. L. 1975 Theoretical investigation of curved pipe flows. Ph.D. thesis, New York State University at Buffalo, 160 pp.

SINGH, M. P. 1974 Entry flow in a curved pipe. *J. Fluid Mech.* **65**, 517–539.

SOH, W. Y. 1983 Laminar entrance flow in a curved pipe. Ph.D. thesis, University of California, Berkeley, 91 pp.

SOH, W. Y. & BERGER, S. A. 1984 Laminar entrance flow in a curved pipe. *J. Fluid Mech.* **148**, 109–135.

STEWARTSON, K., CEBECI, T. & CHANG, K. C. 1980 A boundary-layer collision in a curved duct. *Q. J. Mech. Appl. Maths* **33**, 59–75.

TALBOT, L. & WONG, S. J. 1982 A note on boundary-layer collision in a curved pipe. *J. Fluid Mech.* **122**, 505–510.

YAO, L-S. & BERGER, S. A. 1975 Entry flow in a curved pipe. *J. Fluid Mech.* **67**, 177–196.